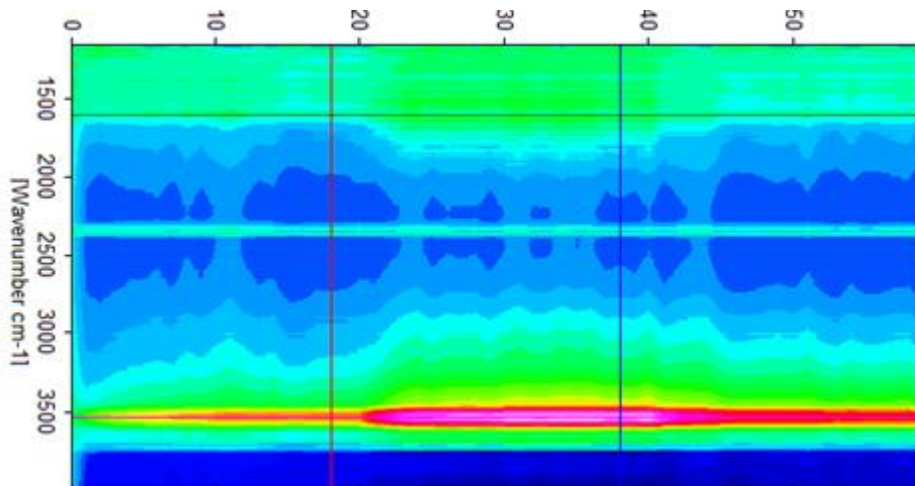# CHALMERS

Methane oxidation over supported palladium and palladium-gold model catalysts

Master's thesis in chemistry and chemical engineering (KBTX12)

Niklas Eriksson

Master thesis report

Methane oxidation over supported palladium and palladium-gold model catalysts

Master's thesis in Chemistry and Chemical Engineering (KBTX12)

Written by: Niklas Eriksson

Supervisors: Per-Anders Carlsson, Peter Velin
Examinator: Hanna Härelind

Department of Chemistry and Chemical Engineering
Chalmers University of Technology
Gothenburg

2018-06-17

Methane oxidation over supported palladium and palladium-gold model catalysts
Niklas Eriksson

Supervisors: Per-Anders Carlsson, Peter Velin
Examiner: Hanna Härelind

Cover: Operando IR 2D contour plot of a palladium on alumina catalyst over the methane oxidation reaction. The colour indicates the intensity of the spectrum where red colour represents high intensity.

Methane oxidation over supported palladium and palladium-gold model catalysts

Niklas Eriksson
Department of Chemistry and Chemical Engineering
Chalmers University of Technology

Abstract

A growing population is in demand of transport and of fuels, especially fuels that are environmentally friendly. Natural gas exists in enormous quantities around the globe making it interesting as a fuel. Methane (CH_4) is the main constituent of natural gas, also of biogas. Methane is however a greenhouse gas and the amount of slipped methane from combustion must be minimized. Palladium catalysts are the most active but suffers from the deactivating problem of water inhibition. Water is a product of the methane oxidation reaction and cannot be avoided. In this project hydrophobic support materials is being investigated as well as palladium-gold alloys as active phase. Catalysts are being synthesized using incipient wetness impregnation and 2 wt% palladium. In the case of the palladium-gold catalysts, a molar ratio of Pd:Au at 1:4 is being used. The samples are characterized using XRD, BET and CO chemisorption. Palladium oxides are shown on the XRD on the Pd/BN and alumina samples. The total surface area of all samples are determined using BET. Pd/Al_2O_3 has the highest of 144 m^2/g followed by the three different palladium-gold samples on alumina all on 87-90 m^2/g. Pd/SiC and Pd/BN have lower surface areas at 25 and 9 respectively.

A DRIFTS setup with operando IR and a coupled mass spectrometer was used to run a water adsorption, a CO-adsorption and a methane oxidation experiment. The water adsorption revealed that palladium on the hydrophobic support materials didn't interact with the water at all. The CO adsorption showed two different bonds between the palladium and the CO of the samples. A linear bond (1Pd-1CO) and a bridged bond (2Pd-1CO). The conversion of CH_4 in the methane oxidation experiment were determined at the temperatures of 350°C and 450°C. At 450°C Pd/Al_2O_3 and Pd/SiC had the most conversion at about 20%. At 350°C Pd/Al_2O_3 had the best conversion. A clear difference between the palladium-gold samples were observed. The $Pd/Au/Al_2O_3$ had a higher conversion than $Au/Pd/Al_2O_3$ and $(Pd+Au)/Al_2O_3$ where the only difference between the samples is the order of the metal added to the sample. The Pd/Al_2O_3 had a higher activity than the palladium-gold samples but with a surface area 60% larger it was expected. The difference in surface area is likely due to the different calcination temperature (500 of the Pd/Al_2O_3 and 800 on the palladium-gold samples). Pd/BN disappointingly showed no activity. Pd/SiC however showed impressive activity with a very low surface area and may be promising as it completely avoided the water inhibition.

Keywords: Methane oxidation, palladium-gold alloy, boron nitride, silicon carbide, operando IR, DRIFTS

Acknowledgements

Table of content

1 Introduction

With a growing population more people are in need of transport and thus for fuel. As oil based fuels get more attention for releasing greenhouse gas emissions alternative fuels are being investigated. A fuel that is increasing in popularity is natural gas. It has huge reserves estimated to 187.1 trillion cubic meters around the globe which makes it attractive to use[1]. Even though it is a fossil fuel, it is considered the only fossil fuel whose share of energy usage is increasing. Natural gas consists of a mixture of hydrocarbons where methane is the main component with 87-97% [2]. Since methane has a hydrogen to carbon ratio of four, the highest of all hydrocarbons it is inherently clean as fuel [3]. As methane is also the main component in biogas, natural gas can function as a bridging fuel for the environmentally friendly biogas which can reach close to zero net emissions.

Methane does however have a negative impact as a greenhouse gas if released in the atmosphere. It is more than 20 times more potent than carbon dioxide [4]. This implies that slipped methane from combustion must be minimized, which means a catalyst must be used. Palladium catalysts have shown to be very efficient for methane oxidation reaction to carbon dioxide and water [5]. The catalyst does however have a downside, it deactivates in the presence of water. Since water is a product of the methane reaction, the exhausts consist of high levels of water. At lower temperatures the methane oxidation is inhibited by water, and at higher temperatures the catalyst suffers from sintering. A low temperature of combustion is more efficient in terms of energy input. In the methane oxidation it is however more susceptible to the water inhibition which becomes a problem [6].

1.1 Aim of the project

The purpose of this master thesis project is to get an understanding of water inhibition in the methane oxidation reaction. This is done by experimenting with palladium on some unconventional hydrophobic support materials and compare them to palladium on alumina which is known to suffer from water inhibition. Palladium-gold as active metal instead of the conventional palladium will be synthesized. They will be evaluated and compared with palladium in the methane oxidation reaction.

2 Background

This section will cover the basics of catalysis, information about catalyst support materials and the methane oxidation reaction.

2.1 Heterogeneous catalysis

Catalysis are divided into homogeneous and heterogeneous catalysis where the difference is whether the catalyst is in the same thermodynamic phase as the reactants or not. This project includes heterogeneous catalysis where the catalyst is in the solid phase and the reactants being the liquid or gas phase. A catalyst allows for an acceleration of a chemical reaction and isn't consumed in the process. The catalyst provides another path for the reaction which may be complex but is energetically favourable. The catalyst creates chemical bonds to the reactants where they can react during different conditions and finally detach the product. In figure 2.1 the difference between a thermal and a catalytic reaction path is shown. The total energy difference of the two paths are the same but the activation energy is considerably lower in the catalytic reaction path [7].

Figure 2.1 displays 2 routes of a chemical reaction. The orange is a catalytic and more complex route and the blue is a non-catalytic route.

Heterogeneous catalysts often consist of an active metal and a support material. The support material prevents agglomeration and sintering as well as reducing the cost of the catalyst since the active metals typically are expensive. The support material is usually a metal oxide which can provide a large surface area for the metal to be distributed on, which is the basics for a good catalyst.

The bond between the catalyst and the reactants should be of appropriate strength meaning not too weak but not to strong. A weak bond would let the reactants go before reacting into the product. A bond too strong would not let the reactants react because they are instead stuck

there. Reactions therefore have different optimal catalyst and finding the best one can be challenging as there are many factors to take into account. A determination of the quality of a catalyst can be done in different ways. How fast it can convert (turnover frequency), how many reactions it can endure before being deactivated (turnover number), that the correct reaction occurs (selectivity) and of course the percentage of the incoming reactants that are transformed (conversion).

$$Xi = n_i(t=0)\text{-}n_i(t)/n_i(t=0) \hspace{3cm} 2.1$$

The conversion is the one that is being investigated in this report and is defined in equation 2.1.

2.2 Catalytic methane oxidation

Total methane oxidation is the reaction of methane and oxygen to produce carbon dioxide and water and can be seen in equation 2.2.

$$CH_4 + 2O_2 = CO_2 + 2H_2O \hspace{3cm} 2.2$$

A combustion of methane is usually done at 1600°C without a catalyst [8]. The reaction can however also be performed at lower temperatures with a catalyst. A total oxidation at a lower temperature is however difficult and requires an efficient catalyst. The reaction conditions in an exhaust system are demanding as methane (400-1500 ppm) is to be reacted in the presence of water (10-15%) and carbon dioxide (15%). So far palladium has shown to be the best catalyst for the methane oxidation in oxygen rich environments which is the case in many exhaust systems [9]. No side reactions are produced which allows the focus to be at optimizing the conversion and reaction temperature. In order to minimize the energy input a lower temperature is preferred. The palladium catalyst does however seem to deactivate at lower temperature due to water adsorption. Since water is a product of the reaction it will always be present and cannot be avoided. The water adsorption is problematic at temperatures <450°C even though the negative effect can be observed at higher temperatures too but to a lower extent. At temperatures higher than 500°C another problem emerges, water assisted sintering. An optimal temperature for the reaction would be 450-500°C or even lower if the water deactivating problem could be dealt with.

In this project the reaction will be performed at 450°C and 350°C, to evaluate the catalysts as well as investigating the water deactivating problem.

2.3 Catalytic materials

A common support material on catalysts is alumina. Alumina (Al_2O_3) is an amphoteric material meaning it can react as an acid as well as a base. Alumina exists in many different phases where ɣ-alumina is the phase that possess good catalytic properties. It has a porous structure with a surface area of up to 300 m^2/g. It can handle the high temperatures required for calcination and is chemically durable. These properties make it a great support material and

explain why it is used for a number of catalytic reactions [10]. Alumina reacts with water creating hydroxyl (OH) groups on the surface. This effect can negate the catalytic activity and to overcome this a more hydrophobic support material can be used.

Boron nitride (BN) is a very hydrophobic material which exists in different forms. Hexagonal BN is the most stable one and is also called white graphite due to its similarity to graphite. The boron and nitrogen atoms are strongly bonded in two dimensional sheets and the sheets are held together using van der Waals forces. It is a light material with its 2.18 g/cm^3 and insoluble in water. A form of BN called boron nitride aerogels can be synthesized using boron nitride nanotubes and nanosheets. This is an interesting material as it is very porous and has a surface area of up to 1050 m^2/g. Boron nitride is a material not widely used in catalysis and its possible application as a support material is unclear [11, 12].

Another hydrophobic support material is silicon carbide (SiC) also known as carborundum. SiC has properties like high thermostability and high mechanical strength. It has a surface area up to 80 m^2/g which is somewhat low as a catalyst support. Because of its excellent properties in high temperatures suggest that it is a viable option in high-temperature gas phase reactions especially with oxygen absence. Silicon carbide is also a very hydrophobic material [13].

The active site is not regulated to be as a single metal and can instead function as an alloy. Palladium-gold alloys are well studied and used in applications such as hydrogen fuel cells, pollution control and selective oxidation reactions [14]. It is especially effective in the form of nanoparticles with a diameter of a few nanometer. The addition of gold to a palladium catalyst can increase the activity, selectivity and stability. Gold is an inert metal and by alloying with the palladium the main role is to isolate the palladium monomer sites. The palladium sites are then exposed to the reactants increasing the activity. The gold has also proven to weaken the bond of palladium and carbon monoxide [15]. The carbon monoxide is a common self-poisoning component for many catalysts and a weaker bond between the carbon monoxide and the palladium reduces the self-poisoning effect.

3 Theory

This section will cover a short theoretic background about the characterization and analyzing instruments that have been used in the project.

3.1 X-ray diffraction

X-ray powder diffraction (XRD) is a method used to determine the crystal structure and atomic spacing of a powder. An X-ray diffractometer consists of three parts; a sample holder, a radiation source and a detector. The radiation source generates monochromatic X-rays which collides with the sample. When the incoming X-rays are reflected and produces a positive interference it satisfies Bragg's law shown in equation 3.1.

$$n\lambda = 2d \sin \theta \qquad (3.1)$$

Where n is a positive integer, the order of the reflection, λ is the incoming wavelength, d in the interplanar spacing distance and Θ is the angle of incoming X-rays. Since the sample is rotated a plot is made out by 2θ angles on the x-axis and the interference on the y-axis. The plot can then be compared to a database if the aim is to determine the crystal structure. Preparations for X-ray powder diffraction are simple, as the only requirements is a fine-grained powder which needs to be crystalline to get a good-looking spectrum [16].

XRD offer a determination of the particle size using equation 3.2, the Scherrer equation. It allows a calculation of the average grain size of the sample.

$$D = K\lambda/\beta cos\theta \qquad (3.2)$$

Here D is the average size, K is a constant shape factor, λ is the wavelength of the X-ray, β is the broadening at half maximum intensity and θ is the bragg angle [17].

3.2 BET

A large surface area is important within catalysis and can be measured using gas sorption and Brunauer-Emmett-Teller method (BET). A sample is treated with a probing gas that physically adsorbs with weak van der Waals forces. The probing gas is adsorbed on the sample without reacting with it and creates a physiosorbed monolayer. The BET isotherm, equation 3.3 below is then used to calculate the specific surface area.

$$\frac{1}{\left[V_a\left(\frac{P_0}{P}-1\right)\right]} = \frac{C-1}{V_m C} \times \frac{P}{P_0} + \frac{1}{V_m C}$$

$$(3.3)$$

Here Va is the volume of adsorbed gas. P_0 is the saturated pressure of adsorbate gas. P is the partial vapor pressure of adsorbate gas. Vm is the volume of adsorbate gas required to create a monolayer. C is a dimensionless constant related to the enthalpy of the adsorption. This equation is linear which allows for Vm to be calculated and at last the specific surface area using the equation below.

$$SSA = V_m * N_A/V_A * A / m \hspace{3cm} (3.4)$$

Where the SSA is the specific surface area (m^3/g), N_AV_A is Avogadro's number per unit of adsorbate gas and A is the area of the adsorbate molecule. Preparations are important before a BET measurement. Outgassing is performed since there can be no other gases or vapor physically adsorbed on the sample in order to obtain an accurate result. Its performed using low pressures and high temperatures, then keep the sample from contact with air and other gases before the experiment starts [18].

3.3 CO chemisorption

Chemisorption is a type of adsorption where a chemical bond is formed between the adsorbate molecule and a surface. The chemical bond is strong and changes the surface structure. The chemical bond does however require an active surface in order to react, which is why it can be used to characterize catalysts. The adsorbate molecule only reacts with the active sites on the catalyst and allows determination of particle size, number of sites, dispersion and surface area of the active metal which is very important properties of a catalyst. Different gases can be used such as hydrogen, oxygen or carbon monoxide which is the best reactant to palladium catalysts. The sample catalyst is prepared by reduction of hydrogen gas at a low pressure. After the preparation known doses of adsorbate gas is pumped onto the sample in order to create a chemisorption isotherm [19].

3.4 Infrared spectroscopy

Infrared (IR) spectroscopy is an analytical technique commonly used for study structures of chemicals using their absorption of infrared radiation. It is a versatile method that can study samples as liquids, pastes, powders, films and gases. Infrared spectroscopy exposes a sample with IR radiation and the amount of absorbed radiation is measured for different wavelengths of infrared light. The translation of the raw data into the actual spectrum can be done using different techniques. Fourier transform infrared spectroscopy is the most common method and can provide high resolution spectra, a good signal to noise ratio as well as quick measurements. The sample absorbs energy from the IR radiation by stretching or bending its internal bonds causing vibration of the molecules. The absorption allows for a spectrum to be constructed of either absorbance or transmittance versus the wavenumbers. A common IR spectrum can be divided into two regions. The fingerprint region (500-1500 cm^{-1}) and the diagnostic region (1500-4000 cm^{-1}). The fingerprint region can contain large amounts of peaks which can be very hard to interpret. The peaks are however unique to each molecule. Above 1500 cm^{-1} the peaks correspond to functional groups of the molecule allowing for a determination of the sample [20].

3.5 Mass spectrometry

A mass spectrometer (MS) is an analytical instrument that sorts out chemicals by their mass to charge ratio. Mass spectrometry has an outstanding sensitivity, low detection limit and great speed. A mass spectrometer consists of three parts; an ion source, a mass analyzer and a detector. The ion source ionizes the sample, producing charged fragments of the sample. The ions are then separated in the mass analyzer by their mass to charge ratio. The mass to charge ratio ions are measured in the detector and a spectrum is constructed of mass to charge ratio versus the intensity. The intensity is proportional to the abundance of the ions. Mass spectrometry can be used as a qualitative analysis by determining the peaks in a spectrum of an unknown sample. MS can also be used as a quantitative analysis as in the case of reaction kinetics. The MS measures pre-determined mass to charge ratios from the product stream of the reaction. The content of the products can then be tracked, and the reaction can be analyzed [21].

3.6 Operando DRIFT spectroscopy

Operando or in-situ spectroscopy is an analysis method that allows a spectroscopic measurement at a catalytic reaction. Operando measurements has increased in popularity the last years. It is likely because of the availability of commercial cells, but also because of the relative ease to carry out an experiment and couple with a spectroscopic method such as x-ray spectroscopy, x-ray diffraction or infrared measurements. Catalysts can be used as a simple form as a powder which avoids the limitation of external transport. Operando measurements makes an analysis of the catalyst surface possible, since the surface species and adsorbents can be measured when a reaction is forthgoing. An instrument that's used for operando measurements is a diffuse reflectance infrared Fourier transform spectroscopy (from here on referred to as DRIFTS). It is a reactor designed so that an IR can be used to measure the gas phase inside the reactor. The design can be seen in figure 3.1 where the IR radiation passes through the reactor chamber. The reactor involves a gas flow through a catalyst bed during controlled heating. The outlet gas is connected to an MS so that the reaction kinetics also can be evaluated [22].
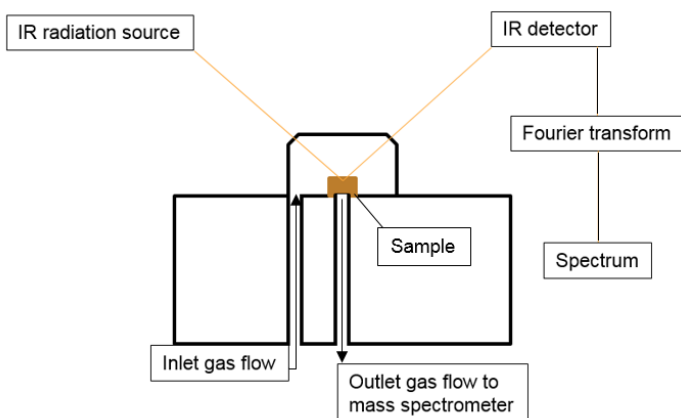

Figure 3.1 is a sketch of a DRIFTS design. The IR radiation interact with the sample inside the reactor. The outlet gas composition is measured by a mass spectrometer.

4 Materials and experimental procedures

In this section the synthesis of the samples will be explained as well as how the experiments including preparations were performed. The experiments of characterization as well as the DRIFTS will be covered as well as a calibration calculation of the MS. The synthesis of the catalysts was done using the incipient wetness impregnation. The samples were characterized using x-ray powder diffraction, BET measurements and CO chemisorption.

4.1 Synthesis of the samples

Incipient wetness impregnation is a common and relatively simple and fast method of synthesis. All samples used in the project were prepared using this method. It requires a support material and a precursor which is mixed and then calcined at a high temperature.

The support materials (Puralox NGA150 Al_2O_3 from Sasol, hexagonal BN 10 micron 99.5% purity from Goodfellow and SiC 1 micron 99% purity from Goodfellow) were weighed and put in a bowl. Palladium precursor ($5\%(NH_3)_4Pd(NO_3)_2$ dissolved in water) were added so that Pd made 2% of the catalyst total in weight. Milli-Q water were then added until the catalyst support was saturated with water. The catalysts were then calcined in either 500°C in 2 hours with a temperature ramp of 1°C per minute. The gold containing samples however were calcined in 800°C in 10 hours with a temperature ramp of 3°C per minute.

The gold was added from the same solution of gold(III)chloride dissolved in water. Gold(III)chloride ($AuCl_4Hx3H_2O$ from Goodfellow) were added to a beaker and dissolved in water. Since all the gold chloride didn't dissolve in the water after heating and stirring the concentration was not determined. A large part of the gold chloride however was dissolved and was used as a gold precursor for the catalysts containing gold. Since all the gold precursor wasn't used, the water was boiled off after the calcinations and the gold was extracted. This allowed for a second estimation of how much gold that was put on the samples. The calculations are shown in table 4.1.

The point of the palladium-gold catalyst is to create particles like the one in figure 4.1. Alumina is the support material which the catalyst mostly consists of.
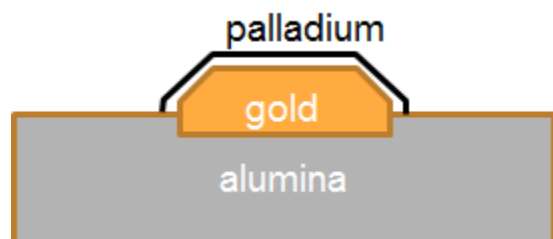

Figure 4.1 is a schematic of the Pd-Au catalyst particles should look like.

The metal particles will have the Pd at the surface supported by the gold. As gold is an inert metal and Pd a very reactive one Pd should of course be on the surface and catalyzing the reaction. The aim was to make the catalysts with a ratio of 4:1 in moles. The other Pd catalysts

contain 2 wt% Pd, naturally the catalysts including gold has the same wt% Pd. For a ratio of 4:1 Pd:Au, a total of 14.8wt% gold is required and will be the aim..

Since Pd/Al_2O_3 catalyst were already synthesized gold were added and the catalyst was called $Au/Pd/Al_2O_3$. At the same time a catalyst where both gold and palladium were added to the alumina was made and called $(Pd+Au)/Al_2O_3$. A gold on alumina was also made and called Au/Al_2O_3. In order for the almost 16wt% gold was to be added on the alumina, several impregnations had to be made and after each impregnation a calcination at 800°C for 10h with a temperature ramp of 3C/min. The amount of gold added to the samples are seen in table 4.1. The weights in the table does not include the lost powder after each calcination, some of the powder get stuck in the bowls or is spilled.

Table 4.1 shows the amount of gold added after each calcination at 800°C for 10h with a temperature ramp of 3C/min as well as a calculation of gold in the samples.

Sample	$(Pd+Au)/Al_2O_3$	Au/Al_2O_3	$Au/Pd/Al_2O_3$
Weight start (g)	1,7	1,7	1,74
Weight after calcination 1 (g)	1,71	1,71	1,75
Weight after calcination 2 (g)	1,75	1,76	1,79
Weight after calcination 2 (g)	1,77	1,77	1,81
Weight after calcination 3 (g)	1,79	1,79	1,83
total gold (g)	0,09	0,09	0,09
wt% gold (g)	5,028	5,028	4,918
Total wt% gold calculated(g)	12.01	12.01	11.76

As the amount of gold on the samples in table 4.1 may not be completely accurate, the remainder of the gold in the gold precursor solution was extracted. After the water was boiled off, the remaining gold in the flask was measured to 0.353g. 2.099g of $HAuCl_4x3H_2O$ were used where the weight percentage of gold is 50.0%. This means that 1.050g of gold was used on the catalysts and 0.353g was left over. 1.050-0.353=0.697g of gold was used on the three samples.

Assuming they got the same amount of gold impregnated which seems to be a good assumption by looking in table 4.1 they each have 0.697/3=0.232g of gold.

There is a sample of gold on palladium/alumina and a sample of gold and palladium added on alumina. In order to get as close to figure 4.1 as possible with palladium on the outside of the catalyst, palladium should be added on top of a gold on alumina sample. This sample was synthesized and called $Pd/Au/Al_2O_3$ and contains 2wt% palladium as the other palladium samples. All the samples made are summarized in table 4.2

Table 4.2 display the samples included in the experiments and their corresponding calcination temperature and wt%

Sample	$Pd/Au/Al_2O_3$	$Au/Pd/Al_2O_3$	$(Pd+Au)/Al_2O_3$	Au/Al_2O_3	Pd/Al_2O_3	Pd/SiC	Pd/BN
Calclination temperature (°C)	800	800	800	800	500	500	500
Active Metals	2wt% Pd 5wt% Au	2wt% Pd 5wt% Au	2wt% Pd 5wt% Au	5wt% Au	2wt% Pd	2wt% Pd	2wt% Pd

All samples were filtered to a particle size between 40 and 80 μm in order to be large enough to not get through the small filter and contaminate the DRIFTS apparatus. A uniform particle size will make sure to obtain more even results.

4.2 DRIFTS experiments

The DRIFTS used was the Vertex 70 (Bruker) using a nitrogen cooled MCT detector and a high temperature stainless steel reaction cell and calcium fluoride windows. It is coupled to a Hidden analytical HPS-20 QIC MS which measures the outlet gas composition.

Before anything can be analyzed, a calibration is needed. The calibration is done on an empty sample and the script used is shown in the table below. It is important to establish a point of zero, and to make sure that the flow is correctly measured. It is done with and without water in order to compensate for the water entering the system. Since methane is close to water in molar mass the methane signal can easily be disturbed by water since the MS measures water at 17 g/mol and methane at 15 g/mol. The difference is small enough to cause a disturbance.

Table 4.1 shows the script used for the calibration. Each step is running 10 minutes. The carrier gas is Argon.

CH_4 concentration	CO_2 concentration	H_2O concentration
0,2		
0,15		
0,1		

0,05		
	0,2	
	0,15	
	0,1	
	0,05	
0,2		2
0,15		2
0,1		2
0,05		2
	0,2	2
	0,15	2
	0,1	2
	0,05	2

An average of each data concentration level is taken and put into figure 4.1 and a linear regression is made. The measured value from the MS is inserted in x from the formula and the output value y is the calibrated value. A plot of the case with methane without water present is shown in figure 4.1 (right).
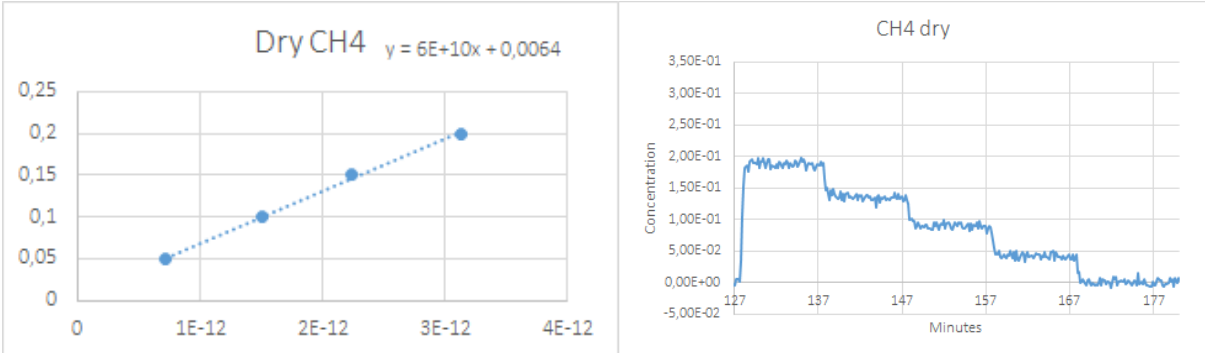

Figure 4.1 (left) displays a linear regression of four different concentrations of methane without any water present. Figure 4.1 (right) displays the levels calibrated to the concentrations on the y-axis.

This was a calibration of methane without water. The same procedure was done applying water as well as for CO_2 with and without water and are displayed in the appendix in figures 9.1, 9.2, 9.3.

The CO adsorption experiment was done at 50°C and 150°C. 0.2% CO was used with argon as a carrier gas for 15 minutes. During this time mass spectrum was running to see that the correct gases were flowing and a spectrum every minute was taken with operando IR. The sample was pretreated with H_2 at 550°C for 20 minutes in order to properly reduce the catalyst surface.

Water absorption was done at 200°C with 2% O_2 and 2% water for 20 minutes using argon as carrier gas. The sample was pretreated with 2% oxygen at 550°C for 20 minutes in order to have an oxidized surface.

CH_4 oxidation was done at 350°C as well as 450°C with a stream of 0.2% CH4 for 60 minutes using argon as carrier gas. After 20 minutes 2% water was turned on and was turned off 20 minutes later. The pretreatment involved an oxidation at 550°C in 2% O_2.

4.3 Characterization instruments and settings

The BET measurements were made on a Tristar 3000, micromeritics. Nitrogen isotherms at 77 K were used. The samples were pretreated by degassing at 498 K for three hours. The surface area was determined from the isotherms.

The x-ray diffractograms were made on D8 Advance, BRUKER AXIS and diffraktometer D5000, Siemens which both used CuKa radiation. The powder was put on a sample holder as a flat surface.

The CO chemisorption was made on a Asap 2020 PLUS, mi micromeritics at 35°C. The samples were pretreated by degassing at 323 K at vacuum pressure for three hours.

5 Results

In this section the results will be presented. Characterizing results from XRD, BET and CO chemisorption measurements followed by the results from the DRIFT. These include some characterization such as CO-adsorption and H_2O-adsorption and then the methane oxidation reaction.

5.1 Characterization results

The surface area of the alumina samples are all quite low except for the Pd/Al_2O_3 sample shown in table 5.1, 145 m^2/g compared to the reference value of 160 of the alumina used [23]. The samples containing palladium and gold has about 90 m^2/g which is significantly lower compared to the Pd/Al_2O_3. Pd/SiC have 25.7m^2/g which is quite low, and Pd/BN are even lower on 9.4. From the XRD graphs shown in figure 5.1 the palladium peaks correspond to facets. Pd/BN and Pd/Al_2O_3 has peaks at 34 (2θ) even though they are barely visible which corresponds to the facet 101. Facet 101 is a favorable facet for palladium oxide [24]. Unfortunately, the XRD graphs are not clear enough on most samples to assign facets.

CO chemisorption was done on the samples Pd/SiC, $(Pd+Au)/Al_2O_3$, $Pd/Au/Al_2O_3$ and Au/Al_2O_3 and the results are presented in table 5.1. The dispersion of Pd/SiC was surprisingly high with 34% compared to the alumina samples. A high dispersion corresponds to a large metallic area and a small crystallite size which is seen in the table. The $Pd/Au/Al_2O_3$ has 12% dispersion, higher than the $Au/Pd/Al_2O_3$ at 5% which indicates that there is a difference between the samples. The Au/Al_2O_3 had an even lower dispersion at 4% but since there is no palladium oxides to adsorb the CO it was expected to be low.

The CO chemisorption instrument was calibrated on palladium using a ratio of 1-1 (linear bond between palladium and carbon dioxide). The Au/Al_2O_3 which does not contain any palladium functions as a reference for the palladium-gold samples. As the Au/Al_2O_3 did adsorb CO with a metal area of 0.39 m^2/g the values of the palladium-gold samples are in reality lower because part of the CO adsorbs on the gold or the alumina instead of the palladium.

Table 5.1 is a summary of the XRD, BET and CO chemisorption experiments performed on the samples.

Sample	Pd/BN	Pd/SiC	Pd/Al₂O₃	Au/Al₂O₃	(Pd+Au)/Al₂O₃	Au/Pd/Al₂O₃	Pd/Au/Al₂O₃
BET Surface area [m²/g]	9.4	25.7	144.7	89.8	90.6	86.6	87.3
Peaks (2θ)	34		34				
Facets	101		101				
Crystallite size using Sherrer equation	-	-	-	-	44	35	28

(nm)							
Dispersion: %	-	33.8	-	4.4	5.4		12.4
Metallic area: m²/(g of sample)	-	3,0	-	0,39	0,48		1.10
Crystallite size hemisphere (nm)	-	3,3	-	25,3	20,6		9.06
Quantity adsorbed (mmol/g)	-	0,027	-	0,016	0,029		0.024

The XRD results are presented as one graph per support material where the different samples are shifted on the y-axis for them to be properly compared. In the case of the alumina, some of the results were normalized in order to fit in the same graph. This was required since different XRD machines were used. Palladium oxide (facet 101) have a peak at 34 2θ degrees which is seen in figure 5.1a in the BN graph. It can also be seen on the palladium-gold samples in figure 5.1c although it is not obvious. In the alumina graph the peaks are observed to be shifted on the x-axis which indicates that an alloy is present. A double peak can however be seen at 67 2θ degrees where the alumina alone shows only one. This peak corresponds to a gold peak of which the particle sizes are calculated using the Scherrer equation.
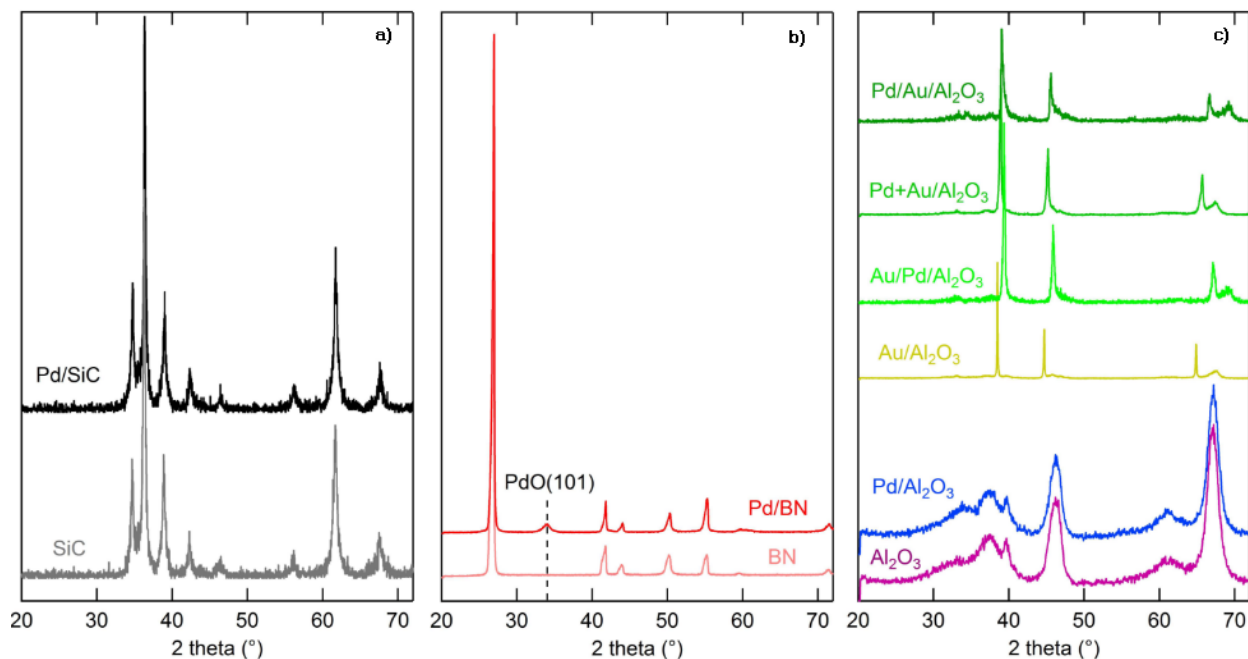

Figure 5.1a) displays the XRD measurement of Pd/SiC compared to the support material SiC over the range of 20-72 2 theta (°). b) Pd/BN compared to BN. c) Pd/Al₂O₃ compared to Al₂O₃ as well as the palladium-gold samples. Different shapes are seen here and are due to the use of different XRD machines.

14

5.2 DRIFTS adsorption measurements

The water adsorption is displayed in figure 5.2. The reference level (0) can be used as the relatively even line at 4000 cm^{-1}. The peaks observed at 3600-4000 represents atmospheric amount of gas phase water and are not to be taken into consideration. As expected the alumina samples adsorbed water which can be seen by the peaks at about 3545 (Pd/Al$_2$O$_3$) and 3490 ((Pd+Au)/Al$_2$O$_3$). The negative peaks can be explained by hydroxyl groups being present even after the pretreatment. As the catalyst is exposed by a relatively large amount of water the vibration of the hydroxyl group shifts to a different frequency. The Pd/SiC and Pd/BN did however not show any peaks which indicates that they did not adsorb any water and did not interact with the water.
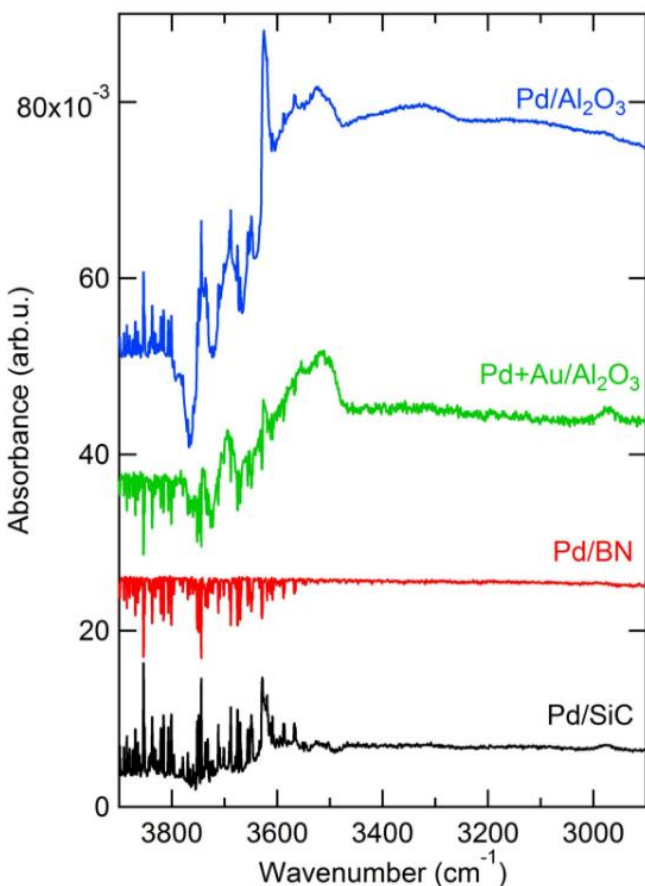

Figure 5.2: Operando IR spectrum during H$_2$O adsorption at 200°C.

Adsorption of CO was made for two different temperatures, 50°C and 150°C. The peaks seen in every single sample between 2050 and 2220 cm^{-1} represents CO in gas phase and are not of any interest. At 150°C in figure 5.3a all the samples except Pd/BN displays clear although broad peaks. The samples consistently have two peaks, these correspond to a linear bond between the palladium and CO as well as a bridged bond. In the case of the linear bond (the lower cm^{-1}), one CO bonds to a single palladium site. The bridged bond (the higher cm^{-1}) requires two palladium sites to one CO. Pd/BN is included also in figure 5.3b at 50°C since it didn't have any peaks at 150°C. Obviously the temperature wasn't the problem since no peaks are found at

50°C either. The experiment did however allow for a comparison of some of the palladium-gold alloys. A notable difference is observed as sample Pd/Au/Al$_2$O$_3$ where the two peaks can be observed. The other palladium-gold alloys shows no response.

A connection can be made between the results in CO adsorption in figures 5.3 and the results from CO chemisorption in table 5.1. The samples are exposed to carbon monoxide in both cases and a good CO adsorption should correspond to a more accurate result of the CO chemisorption. Pd/SiC which had very high dispersion and metal area per gram also displays good peaks in figure 5.3a which makes the result of table 5.1 more confident. The same goes for Pd/Au/Al$_2$O$_3$.
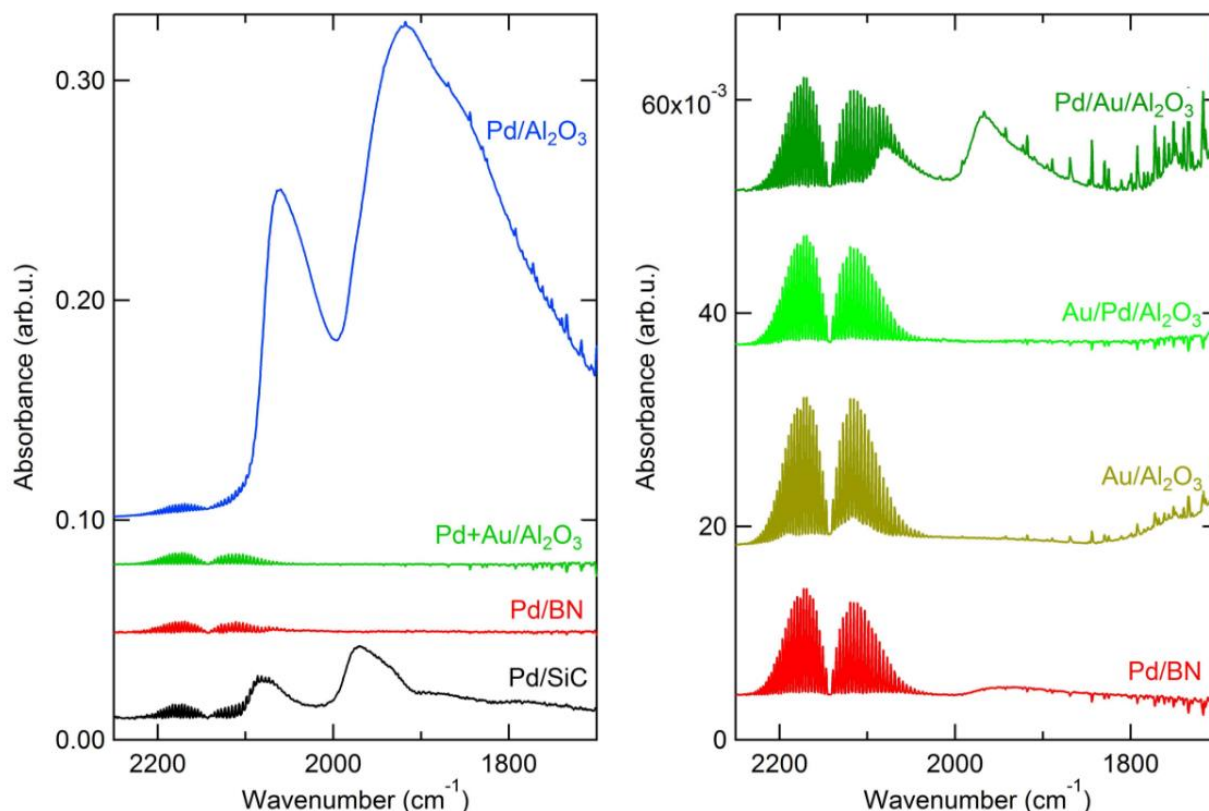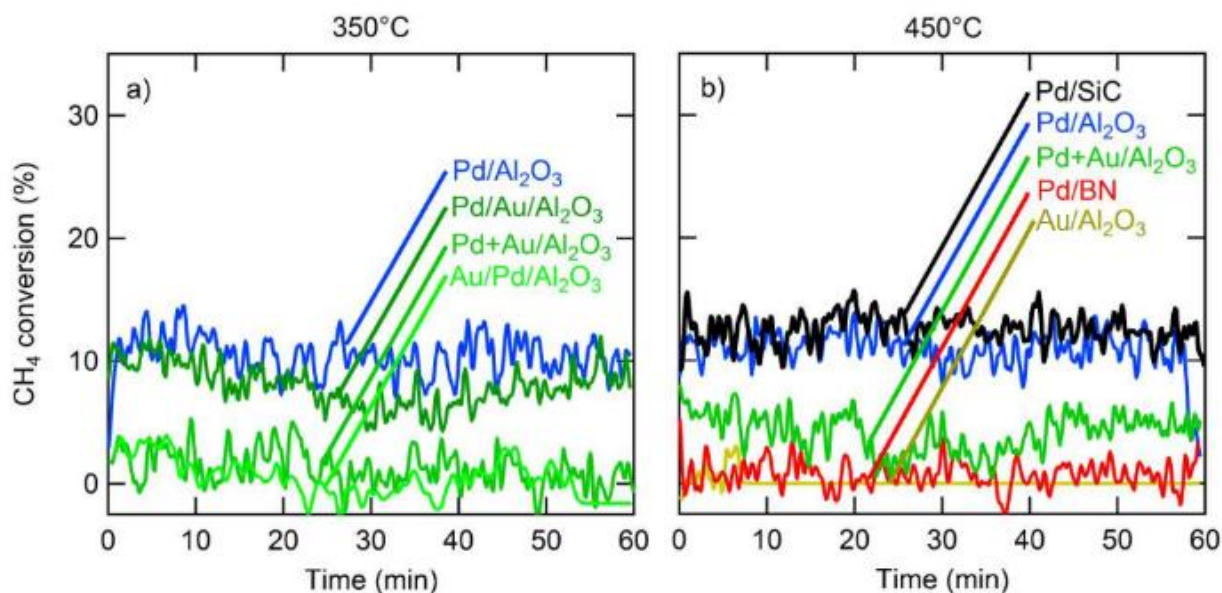

Figure 5.3a) Operando IR spectrum of a CO adsorption experiment at 150°C. b) The same experiment of CO adsorption at 50°C

5.3 DRIFTS methane oxidation

Methane oxidation experiments was performed at the two different temperatures 350 and 450°C in dry and wet conditions. At 450°C Pd/SiC has the greatest conversion at about 13% which is seen in figure 5.5b. Pd/Al$_2$O$_3$ shows a conversion of about 10-13%followed by (Pd+Au)/Al$_2$O$_3$ at 5-7% and Pd/BN and Au/Al$_2$O$_3$ both close to zero. That Au/Al$_2$O$_3$ has a low conversion is not a surprise since gold in itself doesn't have a catalytic activity on the methane reaction. It does however function as a reference since we now can say that it is only the palladium or the palladium-gold alloy that performs the reaction. Pd/BN had disappointingly no conversion, or possibly very low. No obvious change in conversion for the Pd/SiC and Pd/BN can be seen at

the 20-minute mark where the water is turned on which indicates no deactivation of the water. The (Pd+Au)/Al$_2$O$_3$ and possibly also Pd/Al$_2$O$_3$ on the other hand shows a small decline in conversion during these 20 minutes.

Figures 5.5a) shows the methane conversion at 350°C as the percentage of methane converted over 60 minutes. Water is turned on after 20 minutes and turned off at 40 minutes. b) The same methane oxidation experiment at 450°C.

At 350°C in figure 5.5a all the alumina samples are measured. Pd/Al$_2$O$_3$ has the highest conversion in dry as well as wet conditions at about 10-12%. Pd/Au/Al$_2$O$_3$ at 7-10% and the remaining (Pd+Au)/Al$_2$O$_3$ and Au/Pd/Al$_2$O$_3$at 0-4%. A decline at 20 minutes when the water is introduced is observed mainly on the palladium-gold samples as the conversion drops and increases again at the 40-minute mark as the water is removed from the system.

Note that on figure 5.5 it is the total conversion that is being presented. What has not been considered in the graphs are the fact that the samples are of different densities and sample loadings. The loadings are shown in table 5.2 and makes it clear that the alumina samples, all between 69 mg and 73 mg are of very similar loadings. The Pd/BN has a very low density and only 45 mg could be inserted into the sample holder. Pd/SiC had the largest sample loading of 102 mg.

Table 5.2 shows the weight of the loadings for the catalysts used in the methane oxidation experiments at 350°C and 450°C.

Sample	Pd/SiC	Pd/BN	Pd/Al$_2$O$_3$	(Pd+Au)/Al$_2$O$_3$	Au/Al$_2$O$_3$	Pd/Au/Al$_2$O$_3$	Au/Pd/Al$_2$O$_3$
Weight 450°C experiment (mg)	102	45	73	69	70	-	-
Weight 350°C experiment (mg)	-	-	71	70	-	71	70

The operando IR spectra as well as the MS data of Pd/Al_2O_3 are presented in figure 5.6. In figure 5.6b and 5.6d three spectra are presented which all differ. Between 1200 cm^{-1} and 1800 cm^{-1} a lot of peaks are observed especially when water is present. These represent water in gas phase and is not what is in focus. The double peak at 2350 cm^{-1} which all three lines have in common represents CO_2. The CO_2 peak does not only measure the CO_2 in the reaction but also the atmospheric CO_2 which can differ due to other sources than the reaction. The peak of 3500 cm^{-1} can be recognized from figure 5.2 and represents the water bond to the catalyst surface. It is obvious that when the water is turned on it bonds to the Pd/Al_2O_3 sample as it is doubled in intensity. When the water is turned off and the experiment ran for 20 more minutes the peak is decreasing but is not going down to or below the intensity of the dry condition at the start of the experiment. This indicates that the water inhibiting is not reversible, at least not in the time span of the experiment. The 3500 cm^{-1} peak can be followed more closely by looking at figure 5.6a where the intensity (red colour) is substantially increased at 20 minutes and after 40 minutes decreasing slowly. The MS data can be observed in figure 5.6d and although the methane line seem to have a very interesting behavior as it's jumping it's most likely due to the fact that the molar mass of CH_4 and H_2O is similar and the detector can't differentiate between the two, even as it is calibrated. This is the reason some of the data is removed completely as it not important as a result. Methane is measured at 15 and water at 17 g/moles. The CO_2 line however seem to be even which means that the methane is converted evenly during the experiment.
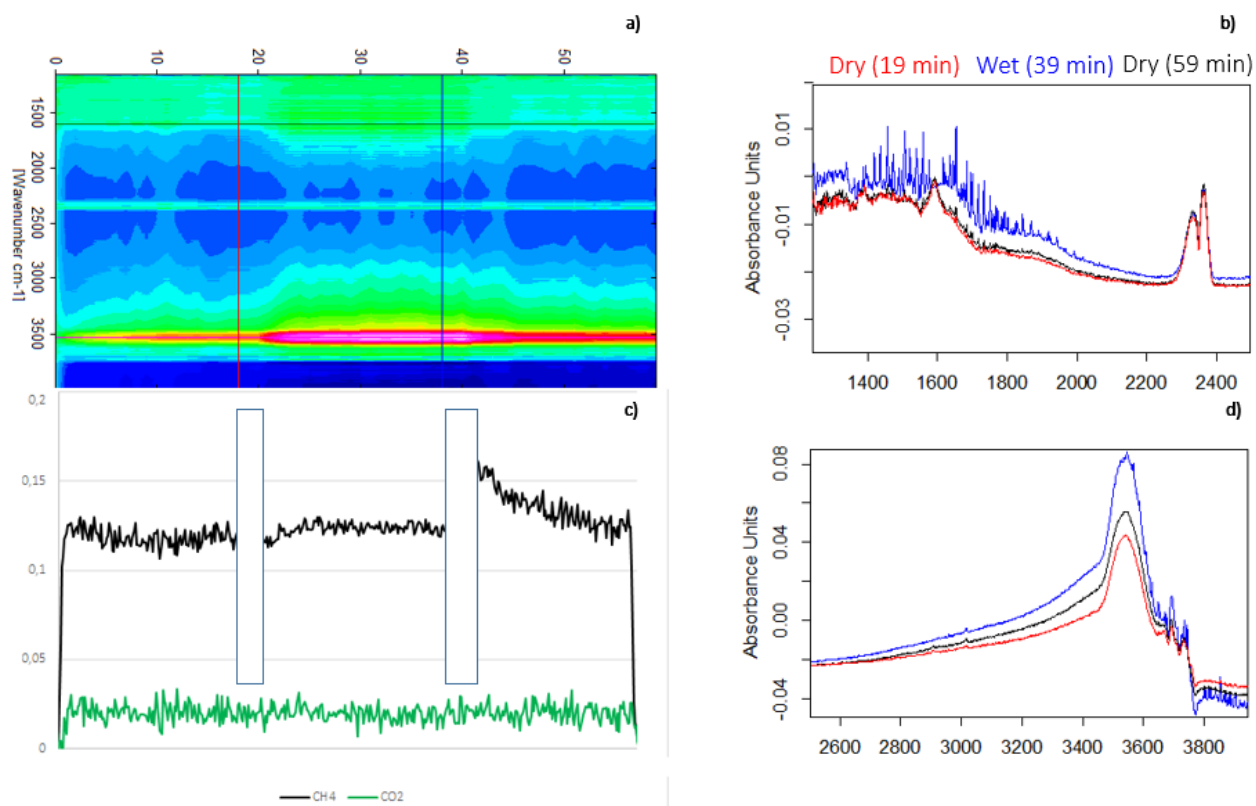

Figure 5.6 shows Pd/Al_2O_3 at 450°C. a) is an operando IR 2D contour of the experiment. The y-axis displays wavenumbers and the y-axis minutes. b) and d) displays 3 IR spectras taken at

different times during the experiment. c) is the MS data from the experiment where the black line represents the methane signal and the green the CO₂.

The operando IR data of the (Pd+Au)/Al$_2$O$_3$ is shown in figure 5.7 and a similar pattern is observed compared to the Pd/Al$_2$O$_3$ sample in figure 5.6. The water adsorbing peak in figures 5.6b and 5.6d at 3500 cm^{-1} increase drastically when water is introduced at 20 minutes (red coloured line) and declines when the water is turned off at 40 minutes (blue coloured line). The intensity of the water adsorbing peak at 60 minutes is almost as low as the one at 20 minutes in figure 5.7d. Conversion is observed during the whole 60 minutes as can be seen in figure 5.7c. It does seem to decrease between 20 and 40 minutes looking at the CO₂ signal, suggesting it is deactivated by the water. The CH$_4$ is once again hard to make anything out of it as it is disturbed by the water signal.
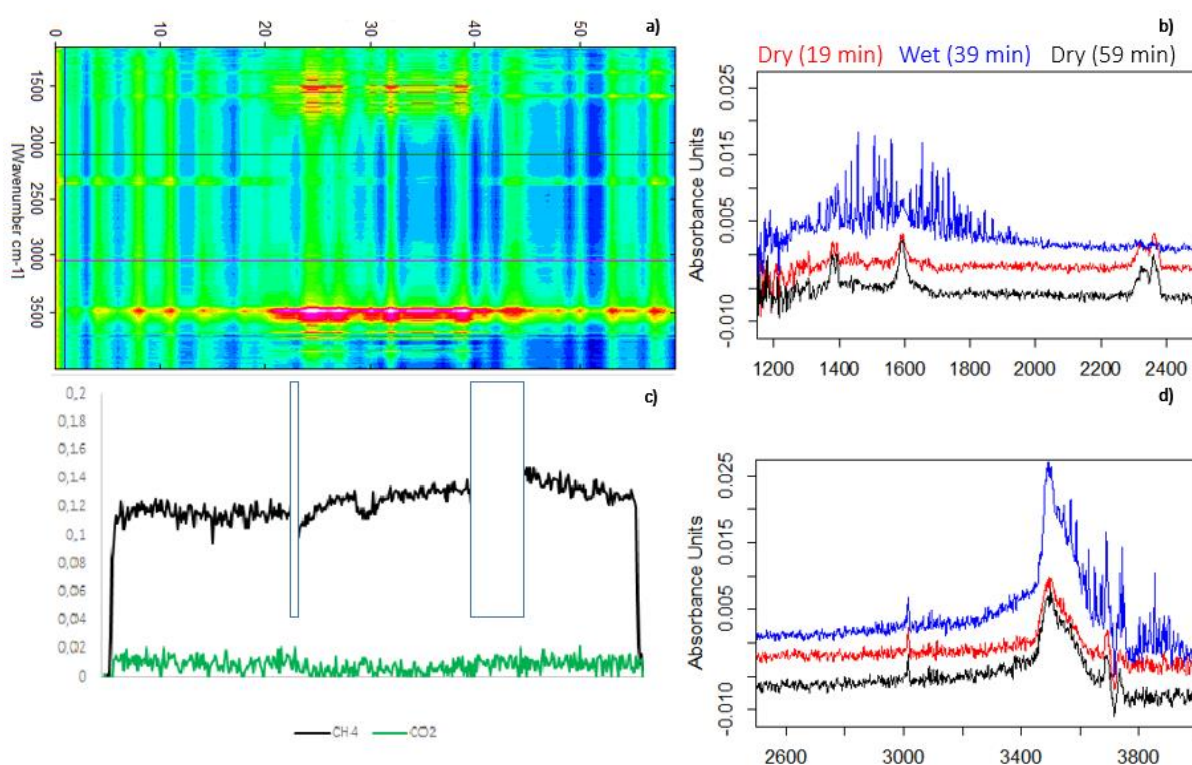

Figure 5.7 shows (Pd+Au)/Al$_2$O$_3$ at 450°C. a) is an operando IR 2D contour of the experiment. The y-axis displays wavenumbers and the y-axis minutes. b) and d) displays 3 IR spectras taken at different times during the experiment. c) is the MS data from the experiment where the black line represents the methane signal and the green the CO₂.

19

No water adsorption is observed for the Pd/SiC sample as there are no peaks at 3500 cm^{-1} in figure 5.8b or 5.8d. The 2D contour in figure 5.8a shows no peaks at all except the CO_2 at 2350 cm^{-1}. The wet spectrum in figure 5.6b shows water in gas phase since the peaks at frequencies 1200-1700 cm^{-1} and 3600-4000 cm^{-1} are present. The CO_2 signal from the MS in figure 5.8c is consistent and does not decrease when water is introduced.
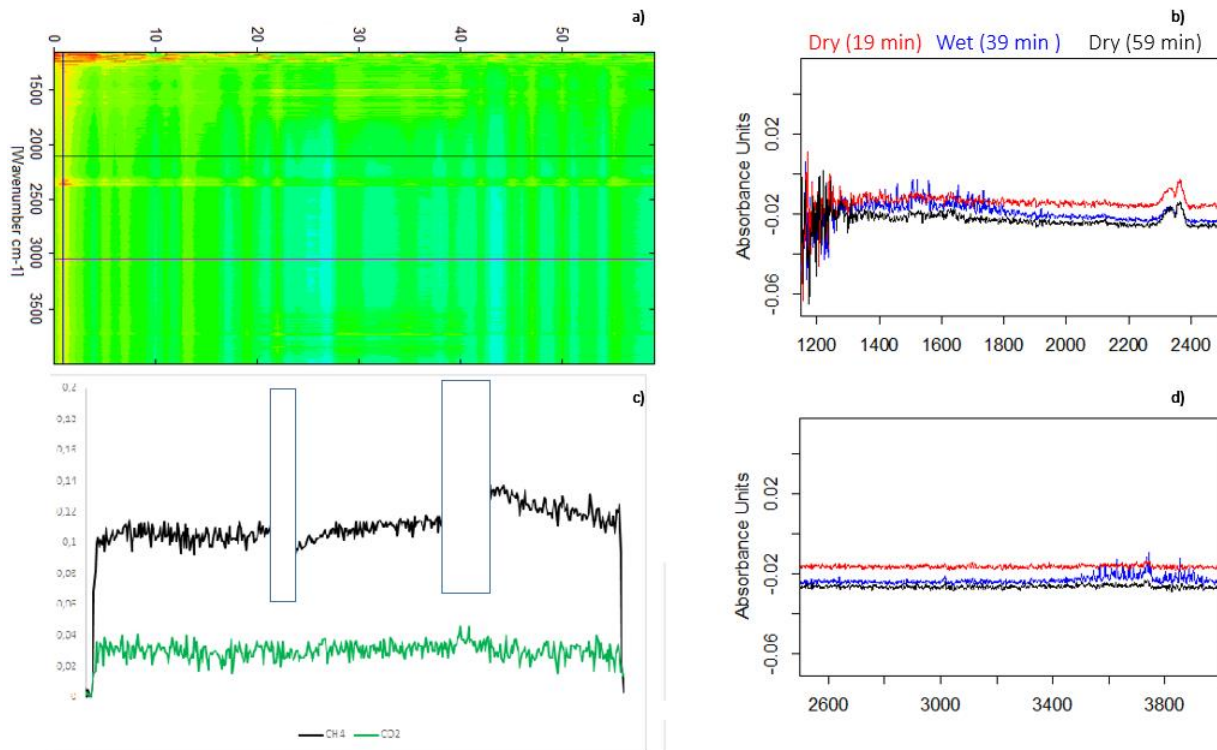

Figure 5.8 shows Pd/SiC at 450°C. a) is an operando IR 2D contour of the experiment. The y-axis displays wavenumbers and the y-axis minutes. b) and d) displays 3 IR spectras taken at different times during the experiment. c) is the MS data from the experiment where the black line represents the methane signal and the green the CO_2.

Pd/BN behaves similar to the Pd/SiC sample looking at the operando IR signals in figure 5.9b and figure 5.9d and also confirmed by the 2D contour in figure 5.8a. The signal after 20 minutes and 60 minutes look very much the same apart from a shift in intensity, even though water is observed in the gas phase. The CO_2 signal in figure 5.9c show little to none conversion.
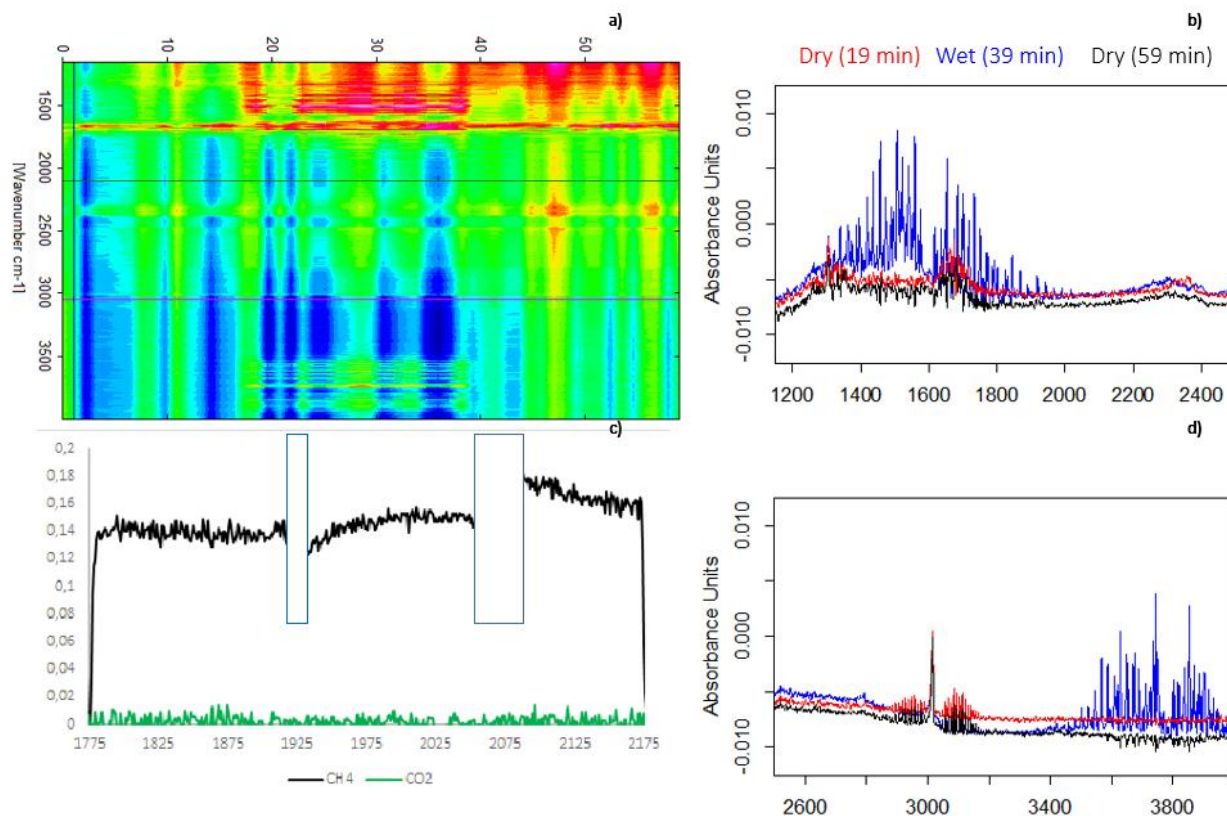

Figure 5.9 shows Pd/BN at 450°C. a) is an operando IR 2D contour of the experiment. The y-axis displays wavenumbers and the y-axis minutes. b) and d) displays 3 IR spectras taken at different times during the experiment. c) is the MS data from the experiment where the black line represents the methane signal and the green the CO_2.

6 Discussion

The surface area of the palladium-gold samples were very similar to each other. Their surface area were however almost half of the palladium sample. This is very likely due to the high calcination temperature of 800°C of the samples containing gold where the palladium sample was calcined at 500°C. It is also possible that the large amount of metals in the palladium-gold samples are clogging the pores of the alumina, reducing the surface area. 500°C is a more optimal calcination temperature by looking at the surface area but not always possible to use. The palladium-gold samples require a higher calcination temperature in order to migrate to the desired structure shown in figure 4.1. The lower calcination temperature of 500°C does at least provide a fair comparison between the different support materials. Pd/BN had a surface area of 9 m^2/g which is very low but may still show some activity. Pd/SiC had a little higher area at 25 m^2/g but is still quite low.

The Pd/SiC sample had surprisingly good results in the CO chemisorption with a dispersion of almost 34% and a metallic area of 3.0 g/m^2. This is a very good indication of activity for the methane oxidation reaction. Pd/Au/Al_2O_3 clearly had the higher dispersion as well as metal area compared to (Pd+Au)/Al_2O_3 which indicates a difference between them. The behavior of the dispersion was also consistent with the crystallite size in CO chemisorption as well as the Scherrer equation calculations made in the XRD. The Scherrer equation showed a larger crystallite size of 44 nm ((Pd+Au)/Al_2O_3), 35 (Au/Pd/Al_2O_3) and 28 nm (Pd/Au/Al_2O_3) and the CO chemisorption showed 20 nm (Au/Pd/Al_2O_3) and 9 nm (Pd/Au/Al_2O_3). It is hard to say exactly how accurate these methods are but it can be noted that the Scherrer particle size is based on the Au peaks in the XRD spectra. Probably the correct particle size is somewhere in between the two results. Pd/Au/Al_2O_3 had a smaller particle size in both measurements which indicates it is the better palladium-gold catalyst. Pd/SiC did have an even smaller particle size according to the CO chemisorption of 3 nm. Unfortunately, the XRD of the Pd/SiC as well as the other samples weren't clear enough to calculate the particle size using the Scherrer equation.

The XRD results of BN as well as SiC are very similar with and without palladium. The lack of palladium on the XRD of Pd/SiC sample is most likely due to the small particle size of 3nm. Palladium is confirmed on the SiC sample as it shows activity in the methane oxidation reaction. Pd/BN does show a small but broad peak at 34 2θ proving palladium on the sample. The same peaks can be found on the alumina samples indicating that an active form of palladium is present on them as well. The palladium-gold samples are other than the peak of 34 2θ very similar to the Au/Al_2O_3 sample. The alloys are however shifted slightly on the x-axis, which could be an indication of palladium or palladium-gold alloy on the samples. The reason Al_2O_3 and Pd/Al_2O_3 is different to the other samples is because of a different XRD machine. Because of a machine malfunction another XRD was used. The changes can be seen in figure 5.1c. The samples were therefore normalized in order to be compared in the same graph.

The water adsorption in figure 5.2 shows that the hydrophobic support materials does not adsorb any water. The Al_2O_3 samples however clearly do which was expected and is now confirmed. The CO adsorption reveals that only some of the samples adsorbs the CO. Pd/Al_2O_3

shows good response and also did Pd/SiC at 150°C. Two peaks are observed at about 1950 cm^{-1} and 2070 cm^{-1} which corresponds to a linear and a bridged bonding respectively. A good response in the CO-adsorption strengthen the results of the CO chemisorption as the adsorption of CO is proved. To be able to see some adsorption on the other samples, the temperature was decreased to 50°C. Two different palladium-gold alloys on alumina were compared and Pd/Au/Al$_2$O$_3$ seems to once again be the better alloy as two broad peaks are observed at a wavelength of about 1950 cm^{-1} and 2050 cm^{-1}.

In the methane oxidation Pd/SiC had surprisingly good result, at 450°C it converted about 15% CH$_4$. It would have been interesting to see the activity of Pd/SiC at 350°C but the test made on the matter was met with technical issues. As the water inhibition becomes larger of a problem at lower temperature Pd/SiC could have shown a high activity with water present compared to the other samples. Pd/SiC had a larger loading size shown in table 5.2 compared to the other samples due to the higher density of silicon carbide. At 350°C the conversions are lower than at 450°C. Judging by the conversion graphs there seems to be a little deactivation of the alumina samples when the water is turned on between 20 and 40 minutes. The observation is more clear on the palladium-gold alloys. This can be explained by the water adsorption in figure 5.2 and also by the IR data of 5.6b and 5.6d for the Pd/Al$_2$O$_3$ and 5.7b and 5.7d for the (Pd+Au)/Al$_2$O$_3$ sample. Water is clearly adsorbed on the samples and when the water is turned off there is clearly some water still bonded to the samples and deactivating them. This behavior is not observed on the Pd/SiC however, the conversion is stable throughout the experiment. The IR data in figure 5.8b and 5.8d shows that a similar spectrum before water is turned on, and after its turned off. At wavenumbers up to 1600 cm^{-1} and above 3500 cm^{-1} peaks of water in gas phase can be observed proving that the water is in fact present. The Pd/BN sample shows the same hydrophobic behavior which proves that the hydrophobic samples does not suffer at all from the water deactivation problem.

An obvious issue that is not included in the graph is of course the weights of the samples. The conversion graphs are not presented as /g but assumes the weights of the sample is the same, this assumption is not true as can be seen in table 5.2. The reason it is still presented as conversion and not conversion/g is due to the simplicity of the graph which shows the direct conversion in % and not just a value. This difference in weight of the sample does of course not take away the impressive activity of Pd/SiC as it had such a low surface area.

A comparison between the palladium sample and the palladium-gold alloy samples are not really fair given they were calcined at different temperatures. As Pd/Al$_2$O$_3$ had more than 50% larger surface area it is very likely going to have a higher activity. This is true as shown in the conversion graphs in figure 5.5. At 350°C the palladium-gold alloys are however not far behind. The water deactivation does seem to be present in both cases. The Pd/Al$_2$O$_3$ seem to have more water adsorbed looking at the H$_2$O adsorption experiment but could be due to having the larger surface area and more palladium at the surface. The activity loss when water is introduced is seen in figure 5.5, especially at 350°C. The palladium-gold samples seem to suffer the most indicating that Pd/Al$_2$O$_3$ is superior. A more fairly conducted investigation would have

to be made to determine whether an alloy of palladium-gold is actually better than palladium alone.

A direct comparison of activity between the different palladium-gold samples are seen in figure 5.5a. The conversions can be compared and clearly $Pd/Au/Al_2O_3$ has the best activity. The $(Pd+Au)/Al_2O_3$ are also having a better activity than $Au/Pd/Al_2O_3$. This indicates that the order of metal put on the support material during the synthesis matters. 800°C were chosen as calcination temperature but how high it would have to be in order for the palladium-gold samples to have the same activity is unclear. It doesn't seem that 800°C was enough for the palladium and gold metals to migrate to the wanted structure in figure 4.1, at least not for the sample where gold were added on top of palladium. When the palladium was added on top of gold on alumina however, the temperature may be able to be reduced in order to gain a larger surface area and thus a better activity. These are subjects of future investigation.

.

7 Conclusions

The hypothesis of avoiding the water inhibition problem in the methane oxidation reaction by using hydrophobic support materials was observed to be true. No indications of any water adsorption can be observed on the catalyst surface at any experiment when palladium on the hydrophobic support materials boron nitride and silicon carbide were used. Pd/BN did not show any activity or at least not nearly enough to be considered good. Pd/SiC however showed some impressive results at 450°C and although a low surface area was measured, a relatively high activity was observed. Continued research on SiC would have to made in order to conclude if it's actually viable, but observations in this project indicates it.

The palladium-gold on alumina samples showed activity in the methane oxidation although not at the level of Pd/Al_2O_3. The palladium-gold alloys did use a higher calcination temperature causing a lower surface area which decreased the activity. Perhaps a lower calcination temperature can be used and a proper comparison can be made.

The palladium-gold samples showed that the order of metal added on the catalyst mattered. The $Pd/Au/Al_2O_3$ where palladium was added on top of Au/Al_2O_3 proved to be the best palladium-gold sample. $(Pd+Au)/Al_2O_3$ where palladium and gold were added at the same time was better than the $Au/Pd/Al_2O_3$ where the gold were added on Pd/Al_2O_3. This indicates that the calcination temperature of 800°C wasn't enough for the metals to reach steady state and migrate to an efficient catalyst.

8 References

[1] World energy council, Energy resources: gas, 2016, [retrieved 2018-02-02], Available:https://www.worldenergy.org/data/resources/resource/gas/

[2] Union gas, chemical composition of natural gas, 2017, [retrieved 2018-02-02], Available:https://www.uniongas.com/about-us/about-natural-gas/Chemical-Composition-of-Natural-Gas

[3] Muhammad Imran Khan, Tabassam Yasmeen, Muhammad Ijaz Khan, Muhammad Farooq, Muhammad Wakeel, Research progress in the development of natural gas as fuel for road vehicles: A bibliographic review (1991–2016), Renewable and Sustainable Energy Reviews Volume 66, Pages 702-741, 2016

[4] Niko M.Kinnunen, Janne T.Hirvi, Kauko Kallinen, Teuvo Maunula Matthew Keenan, Mika Suvanto, Case study of a modern lean-burn methane combustion catalyst for automotive applications: What are the deactivation and regeneration mechanisms?, Applied Catalysis B: Environmental, Volume 207, Pages 114-119, 2017

[5] Joo H.Lee David L.Trimm, Catalytic combustion of methane, Fuel Processing Technology, Volume 42, Issues 2–3, Pages 339-359, 1995

[6] Rahman Gholami, Mina Alyani and Kevin J. Smith, Deactivation of Pd Catalysts by Water during Low Temperature Methane Oxidation Relevant to Natural Gas Vehicle Converters, CATALYSTS, Volume: 5 Issue: 2, Pages: 561-594, 2015

[7] I. Chorkendorff, J. W. Niemantsverdriet, Concepts of modern catalysis and kinetics, WILEY-VCH, 2006. Pages 1-4

[8] Joo H.LeeDavid L.Trimm, Catalytic combustion of methane, Fuel Processing Technology Volume 42, Issues 2–3, April 1995, Pages 339-359

[9] R.BurchP.K.Loader, Investigation of Pt/Al2O3 and Pd/Al2O3 catalysts for the combustion of methane at low concentrations, Applied Catalysis B: Environmental Volume 5, Issues 1–2, 31 December 1994, Pages 149-164

[10] Rahman Gholami ,Mina Alyani and Kevin J. Smith, Deactivation of Pd Catalysts by Water during Low Temperature Methane Oxidation Relevant to Natural Gas Vehicle Converters, *Catalysts* 2015, *5*(2), 561-594

[11] Kiran Y Paranjpe, Alpha, Beta and Gamma Alumina as a catalyst -A Review, The Pharma Innovation Journal 2017; 6(11): 236-238

[12] Yangxi Song, Bin Li, Siwei Yang, Guqiao Ding,Changrui Zhang and Xiaoming Xie, Ultralight boron nitride aerogels via template-assisted chemical vapor deposition, nature Scientific Reports volume 5 Article number: 10337 (2015)

[13] R.Moene, M.Makkee, J.A.Moulijn, High surface area silicon carbide as catalyst support characterization and stability, Applied Catalysis A: General Volume 167, Issue 2, 27 February 1998, Pages 321-330

[14] Mingshu Chen, Dheeraj Kumar, Cheol-Woo Yi, D. Wayne Goodman, The Promotional Effect of Gold in Catalysis by Palladium-Gold, Science 14 Oct 2005, Vol. 310, Issue 5746, pp. 291-293

[15] Mingshu CHEN, D.W.GOODMAN, Promotional Effects of Au in Pd-Au Catalysts for Vinyl Acetate Synthesis, Chinese Journal of Catalysis Volume 29, Issue 11, November 2008, Pages 1178-1186

[16] C. Suryanarayana and M. Grant Norton. X-ray diffraction: a practical approach. 1st ed. pages 63-83, 1998.

[17] The Scherrer Formula for I-Ray Particle Size Determination A. L. PATTERsON Department of Physics, J3ryn Mawr College, Bryn Maser, Pennsylvania (Received July 24, 1939) NOVEM HER 15, 1939 PHYSICAL REVIEW VOLUME 56

[18] Particle analytical, BET, http://particle.dk/methods-analytical-laboratory/surface-area-bet-2/ [retrieved 2018-06-05]

[19] Delft Solids Solutions, Catalyst characterisation by chemical gas adsorption, Available: https://www.solids-solutions.com/rd/porosity-and-surface-area-analysis/catalyst-characterisation-by-chemical-gas-adsorption/ [retrieved 2018-06-05]

[20] Barbara stuart, Infrared spectroscopy: fundamentals and applications, Wiley 2004 pages 1-3

[21] F.A. Mellon, MASS SPECTROMETRY | Principles and Instrumentation, Encyclopedia of Food Sciences and Nutrition (Second Edition) 2003, Pages 3739–3749

[22] F. C. Meunier, Pitfalls and benefits of in situ and operando diffuse reflectance FT-IR spectroscopy (DRIFTS) applied to catalytic reactions, Reaction Chemistry & Engineering issue 2

[23] Sasol, PURALOX®/CATALOX® High purity activated aluminas, Available: http://www.sasoltechdata.com/tds/PURALOX_CATALOX.pdf [retrieved 2018-06-05]

[24] Jutta Rogal, Karsten Reuter, and Matthias Scheffler, Thermodynamic stability of PdO surfaces, Fritz-Haber-Institut der Max-Planck-Gesellschaft, Faradayweg 4-6, D-14195 Berlin, Germany February 2004
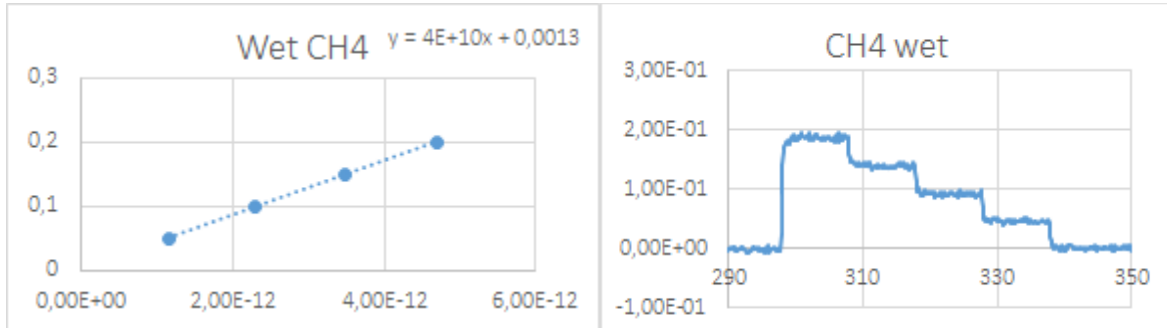
9 Appendix

Calibrations

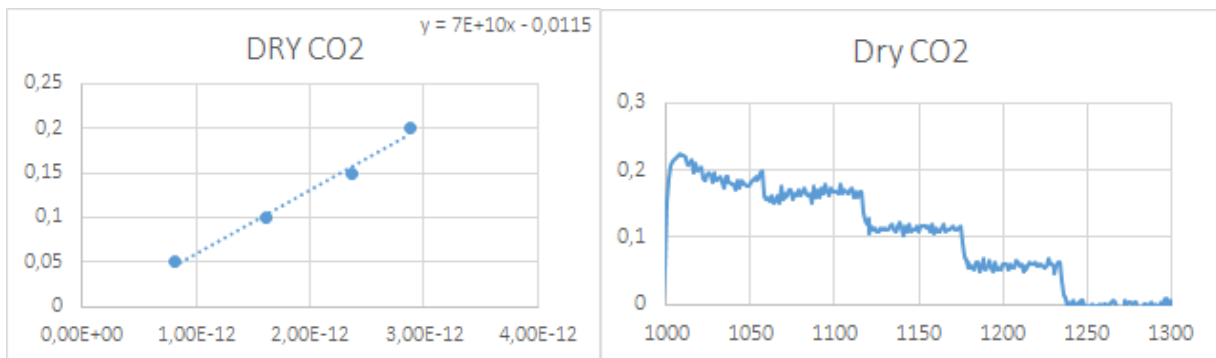*Figure 9.1 shows the calibration used for CH_4 in wet conditions*

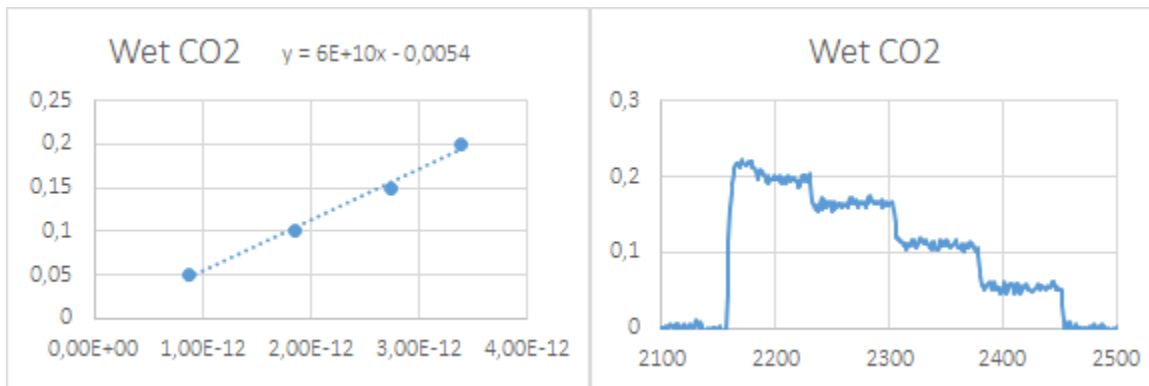*Figure 9.2 shows the calibration used for CO_2 in dry conditions*

Figure 9.3 shows the calibration used for CO_2 in wet conditions